Brillouin Light Scattering and Magnon Wave Vector Distributions for Microwave-Magnetic-Envelope Solitons in Yttrium-Iron-Garnet Thin Films

Hua Xia,* Pavel Kabos,† Hong Yan Zhang, Pavel A. Kolodin, and Carl E. Patton
Department of Physics, Colorado State University, Fort Collins, Colorado 80523
(Received 20 January 1998)

Brillouin light scattering has been used to measure wave number k_m and wave vector $\mathbf{k}_m$ angle distributions for 5 GHz magnetostatic backward-volume-wave envelope solitons in yttrium-iron-garnet thin films. For moderate powers, the data revealed spin waves directly associated with the solitons with k_m values in the ± 300 rad/cm range. For high powers, the data showed high k_m spin waves in the 2500–5000 rad/cm range with discrete in-plane $\mathbf{k}_m$ directions at 90° and other angles around 90° relative to the soliton propagation direction. These high k_m spin waves provide the first direct evidence of spin wave shedding associated with solitons at high powers. [S0031-9007(98)06546-6]

PACS numbers: 76.50.+g, 78.35.+c, 78.70.Gq, 85.70.Ge

Since their discovery by Kalinikos, Kovshikov, and Slavin in 1983 [1], envelope solitons in thin yttrium-iron-garnet (YIG) films have been extensively studied by high frequency techniques. Two recent papers [2,3] list references and summarize the results of these investigations. These measurements utilized microwave techniques only. The solitons were generated through the application of a microwave pulse signal to an input transducer. The pulses propagated along the long and narrow YIG film strip, and the signal was detected by a second output transducer.

This Letter reports a new development in the study of envelope solitons. Brillouin light scattering (BLS) has been used to measure directly the spin wave signals associated with, and generated by, propagating the microwave-magnetic-envelope (MME) soliton pulses. It is shown that one can use a focused laser beam as a probe and BLS as a technique to obtain a signal directly from the localized spin dynamics which make up the soliton. The technique also reveals the presence of additional spin waves which are generated by the soliton. The BLS data yield information on the wave vector makeup of the soliton based spin dynamics.

Previous applications of the BLS technique to nonlinear spin dynamics in magnetic films have provided a critical background to the present accomplishments. First, Kabos *et al.* [4–6] extended the wave vector selective BLS spectrometer concept of Wettling *et al.* [7] and Wilber *et al.* [8] to measure the wave vector distributions of parametric spin waves. Second, Boyle *et al.* [9] and Bauer *et al.* [10] studied two dimensional amplitude profiles for linear and nonlinear cw magnetostatic spin waves in YIG films. The present work shows that the combination of these two techniques allows one to measure BLS signals from spin wave pulses and obtain wave vector distributions for these excitations.

The BLS soliton measurements utilized a 15 mm long, 1.3 mm wide, 7.2 μm thick YIG film with two microstrip transducers placed across the film strip to launch and detect the MME pulse signals as in [2] and [3]. The transducer separation was on the order of a few mm, and the output transducer was movable with respect to the input line. The YIG film was low loss, with a half power ferromagnetic resonance linewidth of 0.6 Oe at 5 GHz.

The MME pulses in the YIG were generated from 14 ns wide microwave pulses at 5 GHz applied to the input transducer. An in-plane static magnetic field of 1090 Oe was applied parallel to the pulse signal propagation direction, in the magnetostatic backward-volume-wave (MSBVW) configuration. These conditions yield a measured pulse group velocity v_g of 3.5×10^6 cm/s and a calculated MSBVW carrier wave number k_m close to 100 rad/cm. In the single soliton regime, the MME pulse steepened and narrowed to a width of about 10 ns.

The microstrip lines used in [2] and [3], for example, were closed single ground plane structures with no possibility for optical access. For the present experiments, the structure shown in Fig. 1 was used for optical access in a forward scattering configuration. The transducer structure with the input and output microstrip lines labeled "In" and "Out" and the long and narrow YIG film strip are on the left side of the figure. The "WP" designates the MME wave packet signal propagated across the structure. The magnetic field **H** is parallel to the strip and the propagation direction.

The open region in the structure provides optical access for the incident 514.5 nm wavelength "Laser" beam with

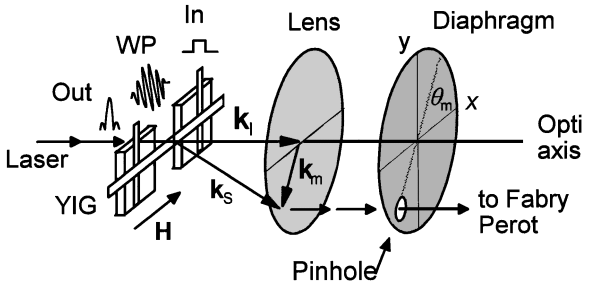

FIG. 1. YIG film transducer structure and optical configuration for wave-vector-selective Brillouin light scattering experiments.

 © 1998 The American Physical Society

wave vector $\mathbf{k}_I$. The beam could be positioned anywhere along the propagation direction from 1.5 to 6 mm from the input transducer. Light of wave vector $\mathbf{k}_S$ is collected by the lens, selected by the diaphragm, and passed to the Fabry-Pérot interferometer (FPI) system.

The lens-diaphragm arrangement provides for wave vector selectivity [4–8]. The diaphragm with a single off-axis pinhole at angle θ_m is shown in Fig. 1 to demonstrate this feature. The pinhole position defines the forward scattering wave vector $\mathbf{k}_S$ analyzed by the FPI system. The in-plane magnon wave vector is then given by $\mathbf{k}_m = \mathbf{k}_S - \mathbf{k}_I$. Rotation of the diaphragm controls the direction of $\mathbf{k}_m$ relative to the propagation direction. The lens focal length of 50 mm, the diaphragm aperture, and the radial position of the pinhole relative to the optic axis control the magnitude of $\mathbf{k}_m$. In the actual experiments, a single diaphragm with one pinhole as shown, a single diaphragm with a slit, and a combination of two slitted diaphragms with one moved off the optical axis were used to select different ranges of $\mathbf{k}_m$ values. One diaphragm with a slit passing through the optic axis and oriented at an angle θ_m, for example, would select the full range of accessible k_m values but only those $\mathbf{k}_m$ directions which correspond to θ_m. With no diaphragms, the maximum k_m was about 9×10^4 rad/cm. With diaphragms, the maximum k_m was about 1.4×10^4 rad/cm. For some measurements, it proved convenient to place a blocking structure on the optic axis to remove low k_m value scattering signals, below 2000 rad/cm, from detection.

The interferometer was a Sandercock high contrast multipass tandem system [11]. The photodetector and photon counting electronics sampled all of the scattered light from the sample and the FPI system. Standard frequency scanned spectra were accumulated with a multichannel analyzer. The count data for the pumped magnon signal at the 5 GHz peaks in the spectra were used to obtain the intensity results presented below.

It is important to emphasize that the BLS signal includes all of the scattering, not just the scattered light during the 14 ns MME pulse passage. It is also important to note that the BLS intensity is related to the magneto-optical parameters of the film, the pumping configuration, and the number of excited magnons. The focus here, however, is on the use of the BLS signal to identify magnon wave vector distributions, rather than the magneto-optic origins of the scattering signal. Such origins have most recently been discussed by Cochran and Dutcher [12].

Figure 2 shows the results of one series of measurements as a function of peak power. The BLS data in (a) were obtained with no diaphragms or blocking structures. The laser was focused on a position on the YIG strip 5 mm from the input transducer. The total scattered light intensity is seen to scale linearly with the input power. The solid line shows a linear fit to the data. This simple and very basic result is remarkable. It indicates that all, or some constant fraction of the input microwave power, goes into the MME signal, and that the light scattering from this transducer

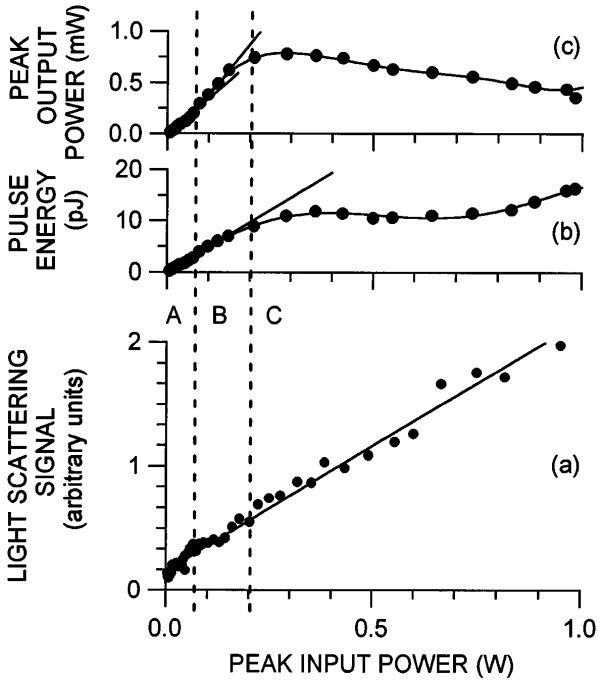

FIG. 2. Light scattering signal (a), integrated output pulse energy (b), and output pulse peak power (c) vs peak input power. For (a), the BLS detection point on the YIG film strip was 5 mm from the input transducer, with no blocking apertures in the optical path. For (b) and (c), the output transducer was also positioned 5 mm from the input transducer.

generated wave packet or other spin waves produced from this wave packet also pick off a *constant* fraction of the total magnon population. As will be evident shortly, there are many spin waves with a wide distribution in $\mathbf{k}_m$ values which are produced in the experiment.

This simple result contrasts significantly with the microwave data in Figs. 2(b) and 2(c). Figure 2(b) shows the integrated pulse energy detected at the output transducer. Figure 2(c) shows the peak power for the same output pulse. The solid curves and lines show spline and linear fits to various parts of the data. These results show that the MME pulse response has a significant dependence on the input power level. The vertical dashed lines and the labels *A*, *B*, and *C* delineate three regions which characterize the MME pulse response [3]. Region *A* corresponds to the linear regime. Region *B* corresponds to a single soliton response. The *B*/*C* boundary corresponds to a fully formed soliton at the output transducer. Region *C* shows the falloff in the response due to multisoliton effects.

The main point of the data in Figs. 2(b) and 2(c), relative to the BLS data in Fig. 2(a), is that the soliton response (i) is definitely nonlinear and (ii) shows a falloff when one moves out of the single soliton regime. Three basic questions are posed by these data: (I) What spin wave modes are associated with the MME pulse signal? (II) Where is the additional spin wave energy going? (III) What additional spin wave modes are generated by or shed from the MME soliton pulse in region *C*?

The data in Fig. 3 address question (I) and, to some extent, question (II). The solid curves provide a guide to the eye for the data. Figure 3(a) shows the light scattering signal obtained with a diaphragm and a single 200 μm diam pinhole. The incident light was focused at a position about 3 mm from the input transducer. The pinhole was positioned along the x axis shown in Fig. 1 and moved across the optic axis in order to scan from negative to positive k_m values at a propagation angle $\theta_m = 0$. This displacement scans the selected k_m values from about -1000 to $+1000$ rad/cm, as indicated. The 200 μm diam pinhole size corresponds to a spread in k_m of about 500 rad/cm. The input power was 200 mW, just at the *B*/*C* boundary in Fig. 2.

The scattering signal shown in Fig. 3(a) is strong only for a range of wave numbers within about ± 300 rad/cm of $k_m = 0$. For the 10 ns soliton pulse width and the group velocity of 3.5×10^6 cm/s, the spatial width of the soliton pulse, Δx_s, is about 0.035 cm. The corresponding spread in k_m, given by $2\pi/\Delta x_s$, is about 200 rad/cm. The data in Fig. 3(a) are clearly skewed toward positive k_m and are consistent with the soliton carrier wave number of 100 rad/cm or so. The width, moreover, is consistent with the expected spread in k_m due to the finite width of the soliton pulse.

The inset of Fig. 3(b) shows additional scattering at moderate k_m values and at θ_m values other than zero degrees. These data were obtained for a crossed slit arrangement, as indicated, to select out both k_m and θ_m. The operating conditions were the same as for Fig. 3(a). This broad scattering in the 1000–2500 rad/cm range of k_m was most pronounced for θ_m near 40°. There was some such scattering at other angles, including $\theta_m = 0$, but $\theta_m = 40°$ yielded the strongest signal. The off-angle result is related to the finite width of the YIG strip and the "snakelike" cw mode profiles recently reported in Ref. [10]. The high k_m values are most likely related to the higher order MSBVW dispersion branches which may be excited by the 50 μm wide input transducer.

The situation changes when the power is increased into region *C*. The data points in Fig. 4 are for an input peak power of 10.5 W, well into region *C*. The solid curves are a guide to the eye for the data. The dashed curve in Fig. 4(b) is for cw microwave excitation and will be considered shortly. The excitation conditions remained the same as above. The BLS detection point was moved back to the 5 mm position to minimize the pickup of the Fig. 3(b) inset spin waves and to see only those modes generated by the soliton at high power. The blocking diaphragm on the optic axis was also used to eliminate the strong low k_m scattering associated with the soliton. The data points in Fig. 4(a) were obtained with a diaphragm which was centered on the optic axis and contained a single 200 μm slit. This diaphragm was rotated to select θ_m only. This arrangement gave, therefore, no additional selection for k_m, so that the BLS signal included spin waves with k_m values in excess of about 2000 rad/cm. For Fig. 4(b), the θ_m selection diaphragm was set at 90° and a second off-axis diaphragm was used to select k_m.

The data in Fig. 4(a) show that with k_m unselected, except for the low k_m block, spin waves are detected over a range of discrete θ_m values with a very strong main peak at $\theta_m = 90°$. There are additional reasonably well resolved peaks at 20°–25° and around 45° to either side of the 90° peak. Keep in mind that the propagating MME soliton wave packet low k_m signal corresponds

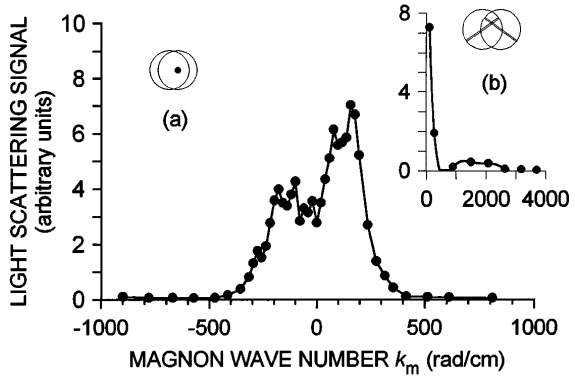

FIG. 3. Light scattering signal as a function of the magnon wave number k_m. The BLS detection point was 3 mm from the input transducer. (a) is for a 200 μm pinhole aperture, $\theta_m = 0$, and an input peak power of 200 mW. (b) is for a double slit arrangement to select out both k_m and θ_m, an input peak power of 205 mW, and $\theta_m = 40°$.

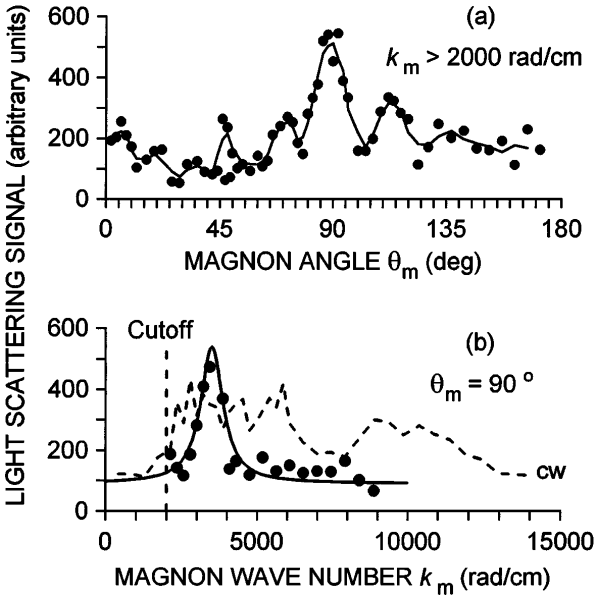

FIG. 4. The data points show the light scattering signal as a function of (a) magnon angle θ_m with k_m unrestricted and (b) wave number k_m at $\theta_m = 90°$. The solid curves are a guide to the eye. The dashed curve corresponds to the k_m distribution obtained for cw excitation and at $\theta_m = 90°$. The BLS detection point was 5 mm from the input transducer and the low k_m block was in place. The input peak power was 1.05 W for the soliton data and 0.502 W for the cw data.

to $\theta_m = 0°$. These high power and high k_m spin wave signals have wave vectors which are centered at a θ_m value which is *perpendicular* to the MME soliton wave vector. Figure 4(b) shows the k_m distribution for the peak in 4(a) at $\theta_m = 90°$. These data reveal a well resolved spin wave peak close to $k_m = 3500$ rad/cm.

Additional data, similar to that shown in Fig. 4(b), were obtained for θ_m values which correspond to the other peak positions in Fig. 4(a). In general, these profiles showed more structure and the range of k_m values for appreciable scattering was somewhat broader than in Fig. 4(b). Still, the predominant scattering was in the 2500–5000 rad/cm range. No spin waves were observed for k_m values above 5000 rad/cm or so.

The existence of spin waves propagating at $\theta_m = 90°$, and other angles away from the soliton propagation direction, demonstrates that the excited modes are not simply due to the reshaping of the propagating soliton. The Fourier components produced from any reshaping would still be at $\theta_m = 0°$. As discussed below, parametric spin waves at $\theta_m = 90°$ but with much broader k_m distributions are obtained under cw excitation conditions. It is clear that the magnons shown in Fig. 4 are nonlinear spin waves produced by the soliton pulse at high power. This is consistent with MME soliton collision experiments [13] which showed clear evidence of a "wake" produced by a propagating MSBVW soliton. It was emphasized earlier that the BLS experiment samples all of the spin waves generated in the film, not just those connected with the passing MME pulse. The Fig. 4 data show that the parametric and possibly the wake spin waves from MME solitons leave a clear BLS signature.

The results in Fig. 4 answer questions II and III above. It is now clear that the multisoliton pulse sheds energy in the form of spin waves with various θ_m values and k_m values in the range of several thousand rad/cm. These modes do not contribute to the detected microwave signal at the output transducer and do not show up through microwave measurements of the sort shown in Fig. 2.

The strong BLS peak at $\theta_m = 90°$ is reminiscent of a similar peak reported for second order spin wave instability processes in YIG films under cw excitation [6]. There, one sharp peak at $\theta_m = 90°$ with a very broad k_m distribution was obtained.

In order to check the connection with those previous results, additional BLS data were obtained under the same conditions as above, except that the pulse width was extended to 30 μs and the peak power was reduced to 502 mW. This power level is still within region *C*, but the wide pulse provides essentially cw excitation. For this experiment, the angle data which corresponds to Fig. 4(a) showed one very sharp BLS peak at $\theta_m = 90°$ and no others, the same as in [6]. The k_m data for the cw case is shown by the dashed line in Fig. 4(b). Here, also as in [6], the data show a very wide distribution in scattering signals. There seems to be a natural evolution as one moves from cw excitation or long pulses to short pulses. The pulse data in Fig. 4 represent the end product of this evolution for MME soliton pulses.

The spin waves generated by the soliton signal at $k_m \approx 3500$ rad/cm and $\theta_m \approx 90°$, etc., have wave vectors which are in-plane and more-or-less perpendicular to the soliton carrier wave vector. Spin waves with these k_m and θ_m values, and at the soliton carrier frequency, are peculiar to the dipole exchange modes found only in the thin film limit. The spin waves identified here are not allowed modes in bulk YIG. This is the same situation found in [6]. The present data show that the spin wave modes shed by MME multisoliton excitations must be analyzed in terms of the full dipole-exchange formalism for thin films.

This work was supported in part by the U.S. Army Research Office, Grant No. DAAH04-95-1-0325, and the National Science Foundation, Grant No. DMR-9400276. The YIG film was grown by Dr. J. D. Adam, Northrop Grumman Science and Technology Center, Pittsburgh, Pennsylvania. Professor B. A. Kalinikos and Professor A. N. Slavin are acknowledged for helpful discussions.

*Permanent address: National Laboratory of Solid State Microstructures, Nanjing University, Nanjing 210093, China.

†On leave from the Slovak Technical University, Bratislava, Slovakia.

[1] B. A. Kalinikos, N. G. Kovshikov, and A. N. Slavin, JETP Lett. **38**, 413 (1983).

[2] B. A. Kalinikos, N. G. Kovshikov, C. E. Patton, E. S. Wright, and J. M. Nash, Phys. Rev. B **54**, 15 210 (1996).

[3] H. Xia, P. Kabos, C. E. Patton, and H. Ensle, Phys. Rev. B **55**, 15 018 (1997).

[4] P. Kabos, G. Wiese, and C. E. Patton, Phys. Rev. Lett. **72**, 2093 (1994).

[5] P. Kabos, M. Mendik, G. Wiese, and C. E. Patton, Phys. Rev. B **55**, 11 457 (1997).

[6] P. Kabos, C. E. Patton, G. Wiese, A. D. Sullins, E. S. Wright, and L. Chen, J. Appl. Phys. **80**, 3962 (1996).

[7] W. Wettling, W. D. Wilber, P. Kabos, and C. E. Patton, Phys. Rev. Lett. **51**, 1680 (1983).

[8] W. D. Wilber, J. G. Booth, C. E. Patton, G. Srinivasan, and R. W. Cross, J. Appl. Phys. **64**, 5477 (1988).

[9] J. W. Boyle, S. A. Nikitov, A. D. Boardman, J. G. Booth, and K. Booth, Phys. Rev. B **53**, 12 173 (1996).

[10] M. Bauer, C. Mathieu, S. O. Demokritov, B. Hillebrands, P. A. Kolodin, S. Sure, H. Dötsch, V. Grimalsky, Y. Rapoport, and A. N. Slavin, Phys. Rev. B **56**, R8483 (1997).

[11] Fabry-Pérot interferometer system manufactured by JRS, Ltd., Zwillikerstrasse 8, 8910 Affoltern a. A., Switzerland.

[12] J. F. Cochran and J. R. Dutcher, J. Magn. Magn. Mater. **73**, 299 (1988).

[13] N. G. Kovshikov, B. A. Kalinikos, C. E. Patton, E. S. Wright, and J. M. Nash, Phys. Rev. B **54**, 15 210–15 223 (1996).